Electronic Supplementary Material for

Structural studies on dinuclear ruthenium(II) complexes that bind diastereoselectively to an anti-parallel folded human telomere sequence

Tom Wilson, Paulo J. Costa, Vítor Félix, Mike P. Williamson, Jim A. Thomas

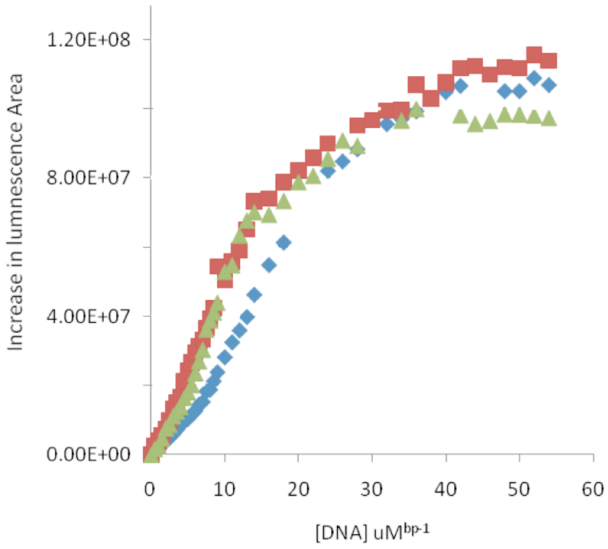

Figure S01 – Luminescence response of ΛΛ-**2**, ΔΔ-**2**, and an unresolved diastereomeric mixture of **2** to the progressive addition of CT-DNA. Red: ΔΔ, green: ΛΛ, blue: diastereomeric mixture, ΛΛ:ΛΔ:ΔΔ 1:2:1.

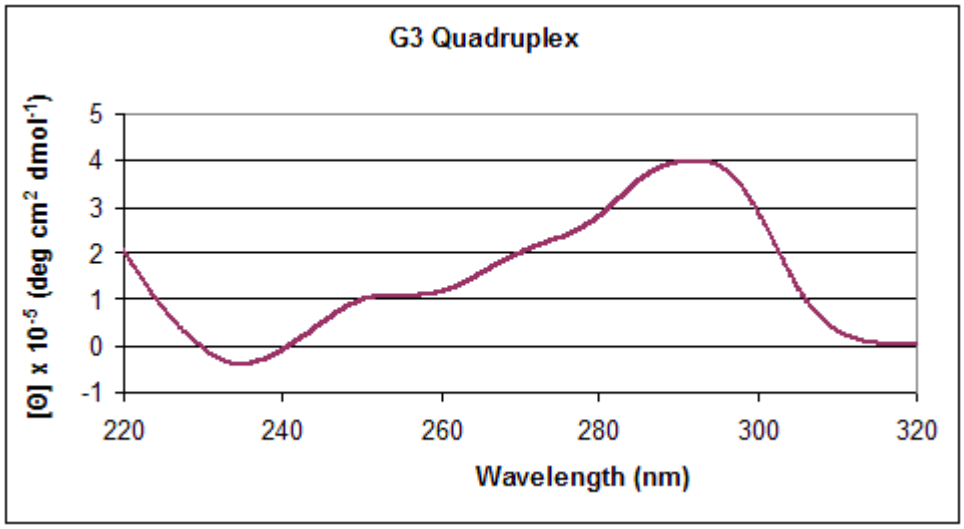

Figure S02. Circular dichroism spectrum of HTS quadruplex. The spectrum was recorded on a Jasco J-810 Spectrophotometer, equipped with a Peltier variable temperature controller, at a rate of 100 nm/min from 200 nm to 320 nm.

Table S1. NMR assignments of the HTS quadruplex

	NH1	NH2/H2	H8/H6	CH3	H1'	H2',2"	H3'	H4'	H5',5"

						2.19,			3.52,
A1			7.98		6.03	2.66	4.74	4.11	3.59
						2.48,			4.11,
G2	11.61		7.74		5.48	2.90	4.95	4.19	4.21
						2.69,			4.15,
G3	10.67	9.71, 6.86	7.51		5.88	2.52	4.98	4.22	4.15
		10.24,				2.92,			4.22,
G4	10.74	6.64	7.98		5.95	2.22	5.04	4.45	4.17
						2.54,			
T5			7.62	1.92	6.34	2.54	4.84	4.22	4.14,
						1.12,			4.10,
T6			7.15	1.89	4.61	1.26	4.45		4.02
						2.53,			
A7			8.11		6.20	2.66	4.59	4.58	3.26,
		10.25,				3.08,			
G8	11.98	6.89	7.28		5.94	2.51	4.87	4.42	4.16
						2.95,			
G9	11.69		8.41		5.59	2.62	5.21	4.43	
						2.67,			4.07,
G10	11.08	9.73, 7.35	7.90		6.32	2.67	5.40	4.31	4.38
						2.13,			4.13,
T11			7.68	1.91	5.64	2.23	4.51	4.21	4.06
						1.15,			3.45,
T12			7.00	1.51	5.56	1.33	3.78	3.64	3.45
						2.66,			3.75,
A13			7.92		5.88	2.60	4.74		3.57
						2.73,			4.01,
G14	10.85	9.75, 6.70	8.01		6.37	2.88	5.04	4.51	4.12
						3.41,			4.47,
G15	11.18	8.61, 6.84	7.23		5.97	2.76	5.17	4.49	4.03

						2.68,			
G16	11.38		7.46		5.95	2.68	5.24	4.26	4.38,
						2.47,			4.26,
T17			7.99	2.06	6.47	2.60	5.06	4.57	4.47
						1.30,			4.06,
T18			7.58	1.85	5.75	2.00	4.87	4.27	4.09
						3.00,			3.82,
A19			8.44		6.31	2.85	5.13	4.44	4.06
						3.49,			
G20	11.28	9.07, 7.56	7.38		6.08	2.91	5.07	4.47	4.33
		9.40,				2.56,			
G21	11.30	6.36	7.46		6.21	2.72	5.06	4.47	
						3.31,			4.39,
G22	11.00	8.82, 6.30	7.91		6.34	2.40	4.74	4.35	4.10

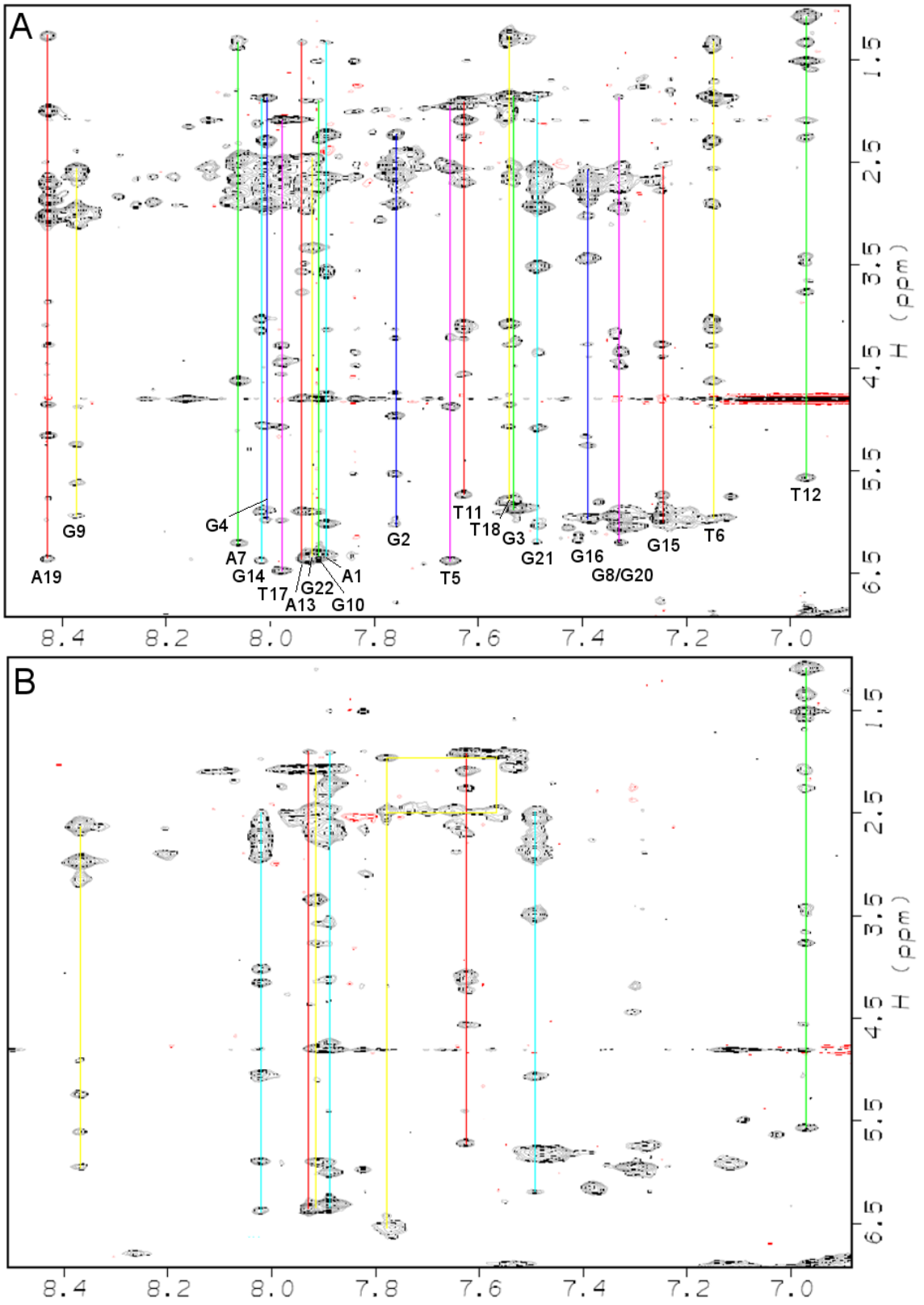

Figure S03. Sections from NOESY spectra of (A) HTS alone, and (B) HTS after addition of one equivalent of ΔΔ-**2**, 50 mM NaCl, pH 7.0, 10 ˚C. The vertical lines show positions of

aromatic protons from different bases as indicated. The signals from the bases shown in red in Fig. 3 are missing in (B). The yellow box for T18 shows a possible exchange doublet.

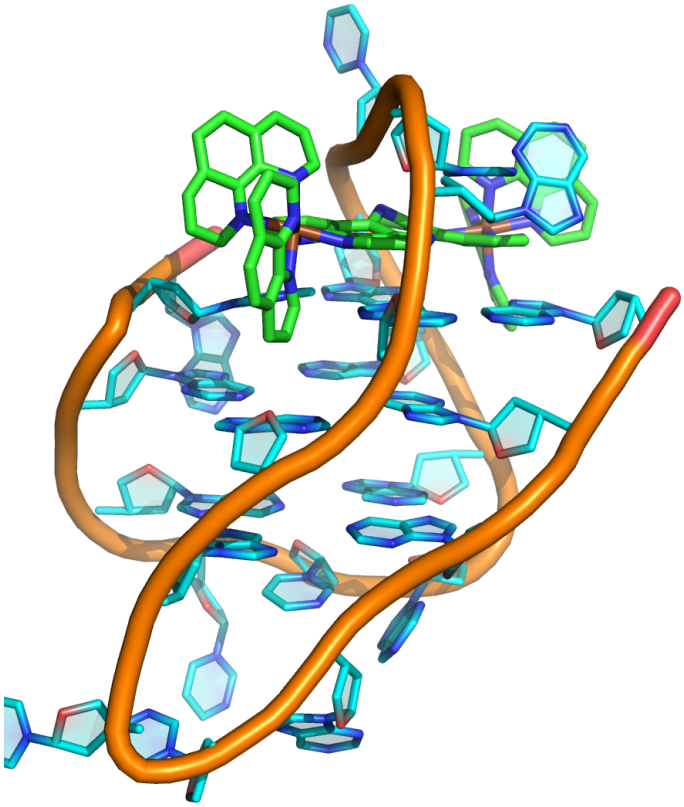

Figure S04. Model of ΛΛ-**2** bound to the HTS, produced using the same parameters as used to produce the ΛΛ-**1** model (Figure 6).

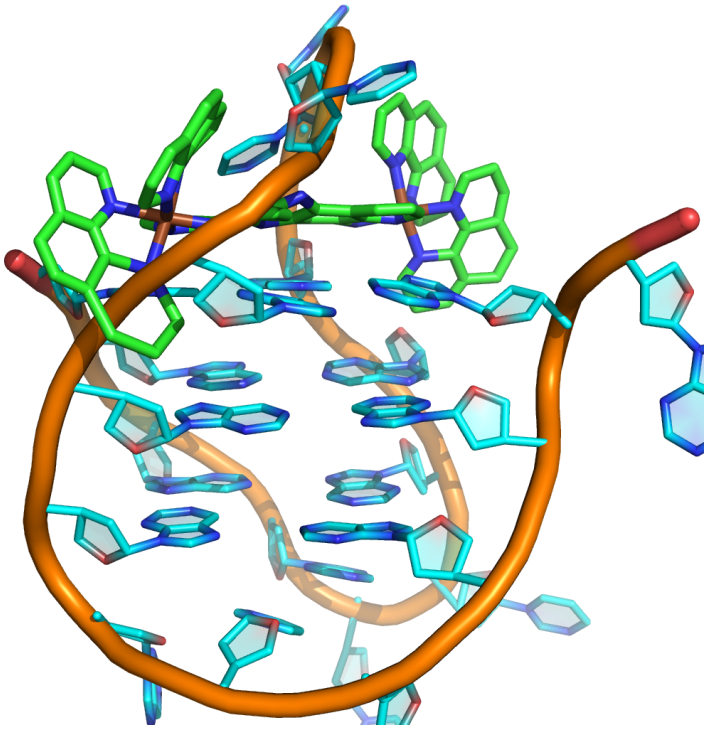

Figure S05. Model of ΔΔ-**2** bound to the HTS, produced using the same parameters as used to produce the ΔΔ–**1** model (Figure 7).

Unconstrained Molecular Dynamics Simulations:

Parameterization of ΛΛ-1 and ΔΔ-1 complexes. For both complexes the X-ray structure reported by Gourdon and co-workers[1] (CSD code ZELCIC) was used as template. Afterwards, both complexes were geometry optimized with Gaussian 03[2] at the Density Functional Theory (DFT) level of theory using the hybrid B3LYP functional.[3, 4] Ruthenium was described by the standard LANL2DZ with associated ECP[5-7] augmented by an *f* polarization function (exponent 1.235)[8] while for the remaining elements the 6-31G(d) basis set was employed. The optimized geometries were then used to calculate the RESP atomic charges by fitting the electrostatic potential obtained at the HF/6-31G*,LANL2DZ(*f*) using 4 concentric layer of points per atom and 6 points per unit (Gaussian IOP 6/33=2, 6/41=4, 6/42=6), post-processing the

Gaussian03 output with the Antechamber module of AmberTools12.[9] Since both ruthenium atoms of the dinuclear complexes are buried inside the molecular surface of the complex and therefore away from the points of the ESP surface for which the RESP charges are computed, direct calculation of ruthenium RESP charges is not advisable and, in order to overcome this issue, the charges on the metal were fixed to their Mulliken values (1.420) during the fitting procedure.

Force field parameters for the bpy and tppz ligands, including bond, angle, torsion, and van der Waals terms were taken from the General Amber Force Field (GAFF)[10] while the octahedral ruthenium coordination sphere of ΛΛ-**1** and ΔΔ-**1** complexes was described with force field parameters mainly adapted from the work of Per-Ola Norrby *et al.*,[11] and later used by Rothlisberger *et al.* to study the solvation of the $[Ru(bpy)_3]^{2+}$ complex in water through classical molecular dynamics (MD) simulations.[12] These extra parameters are summarized in Table S2

Table S2 Force Field parameters for the ruthenium coordination sphere in ΛΛ-**1** and ΔΔ-**1** complexes.

Bond lengths[a)]	r_{eq} (Å)	K_r (kcal mol^{-1} Å^{-2})	
Ru-N	2.081	268	
Bond angles[a)]	θ_{eq} (º)	K_θ (kcal mol^{-1} rad^{-2})	
Ru-N-C	123.5	103.6	
N-Ru-N (*cis*)	91.1	81.25	
N-Ru-N (*trans*)	180.0	24.49	
Dihedral angles[a)]	$V_n/2$ (kcal mol^{-1})	γ	***N***
Ru-N-C-C	1.21	0	-2
Ru-N-C-C	1.41	180	0
Ru-N-C-H	5.27	180	2
N-Ru-N-C (*cis)*	0.25	180	4
N-Ru-N-C (*trans)*	All set to zero		
Van der Waals [b)]	***r*** (Å)	ε (kcal mol^{-1})	
Ru	2.9630		

[a)] Parameters taken from ref.[11]; [b)] Van der Waals terms obtained from ref. [13].

MD Simulation.

Simulations with the free human telomere sequence (HTS), d[$AG_3(TTAG_3)_3$], were performed using the structures reported in Figures 5, 6 and 7 of the Main Text as starting models, removing the ruthenium complexes, and are henceforth labelled **A**, **B**, and **C**. The systems **A**, **B**, and **C** were neutralized by the addition of Na^+ counter-ions described by parameters from Joung and Cheatham's work.[14, 15] Three of these cations were manually placed in the middle of the tetrads. The neutralized models were then solvated in a periodic TIP3P[16] water box with a minimum 10 Å radius distance from the solute atoms.

Subsequently, these three HTS solvated systems were equilibrated using the following multistage simulation protocol: the water molecules and the Na^+ cations (apart from those inside the HTS) were relaxed by Molecular Mechanics (MM) minimization keeping the DNA and the three Na^+ fixed by means of a positional restraint (1000 kcal $mol^{-1}Å^{-2}$). Subsequently, these cations were also allowed to relax together with the solvent and the remaining counter-ions. The third step consisted of a full MM minimization of the entire system. The systems were then heated to 300 K during 50 ps using the Langevin thermostat with a collision frequency of 1 ps^{-1} in an NVT ensemble keeping the DNA fixed with a weak positional restraint (10 kcal mol^{-1} $Å^{-2}$). The heating stage was followed by a 5 ns equilibration period in a NPT ensemble at 1 atm with isotropic pressure scaling using a relaxation time of 2 ps. Data were collected for the subsequent 50 ns for each system leading to a total sampling time of 150 ns for the free HTS solvated structure. The SHAKE algorithm[17] was used in all simulations to constrain all bonds involving hydrogen atoms, thus allowing the usage of a 2 fs time step. A 10 Å cut-off was used for the non-bonded van der Waals interactions.

The interaction of ΛΛ-**1** with HTS was investigated using the structure reported in Figure 6 of the main text as starting geometry, which was neutralized and solvated as

previously reported for the free HTS systems. The simulation protocol was also identical, keeping the ΛΛ-**1** complex and DNA restrained through the first MM minimization stage and in the heating phase.

In order to evaluate the effect that ΔΔ-**1** causes on the quadruplex structure when located under the diagonal loop, simulations with that isomer interacting with DNA were also performed. The structure reported in Figure 7 of the main text could not be directly used given the reported clashes and the fact that the phosphate backbone passes through the middle of one bipy ring. Therefore, the starting structure was generated from the ΛΛ-**1** DNA association (Figure 6, main text), placing the ΔΔ-**1** complex under the diagonal loop and superimposing the ruthenium atoms and the tppz ligand of ΔΔ-**1** to the positions occupied by the ΛΛ-**1** complex, subsequently deleting the latter complex. In these circumstances, only the spatial disposition of two $Ru(bipy)_2$ entities was changed to that of the respective diastereomeric arrangements**.** The remaining simulation details were similar to the ones used for the simulations performed with ΛΛ-**1** complex.

Discussion: Extended MD Simulations

Free HTS, d[AG$_3$(TTAG$_3$)$_3$], simulations. The conformational stability of free HTS solvated structures (systems **A**, B or **C**) throughout the course of the simulation was accessed by monitoring the root mean-square deviation (RMSD) over the simulation, using the respective unrelaxed NMR starting structure as reference (Fig. S06). The initial jump of the RMSD values in all simulations is normal and a consequence of the consecutive MM minimizations used to relax the system before the heating (50 ps), equilibration (5 ns) and collection (50 ns) MD runs. The G-tetrads are held by hydrogen bonds and their RMSD values are low, indicating a minor conformational

rearrangement as expected. On the other hand, the diagonal loops, defined by the G:A:T:T:G residues, experienced a larger rearrangement compared with the starting structures. Furthermore, the RMSD values for the entire HTS structure ("all atoms" in Fig. S06) follow the trend observed for the diagonal loops. In simulation **A**, the system clearly deviates more from the reference structure while simulation **C** yields lower RMSD values, being much closer to the starting structure. This similarity can be seen pictorially in Fig. S07 obtained by overlapping the respective reference structure with a representative conformation from the MD simulation, which was the representative frame from the most populated cluster obtained by clustering the data collection trajectory.

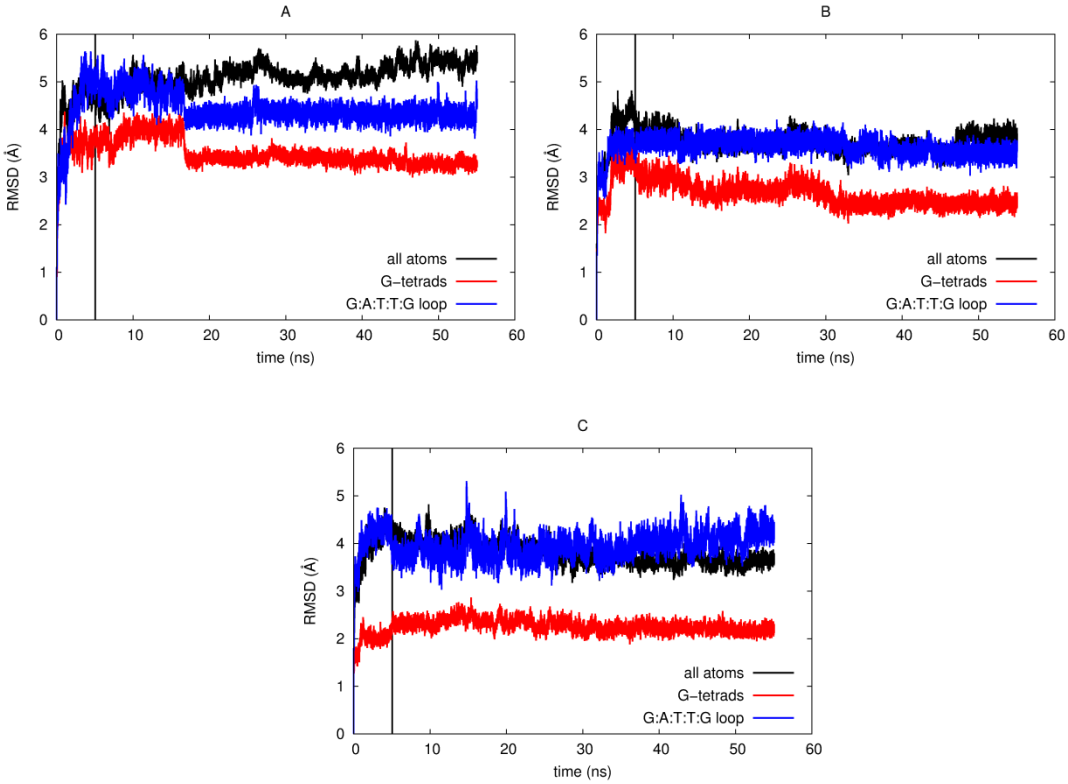

Figure S06 Variation of the RMSD values during the MD simulations **A**, **B**, and **C**. The vertical black line marks the separation between the predefined equilibration and collection stages.

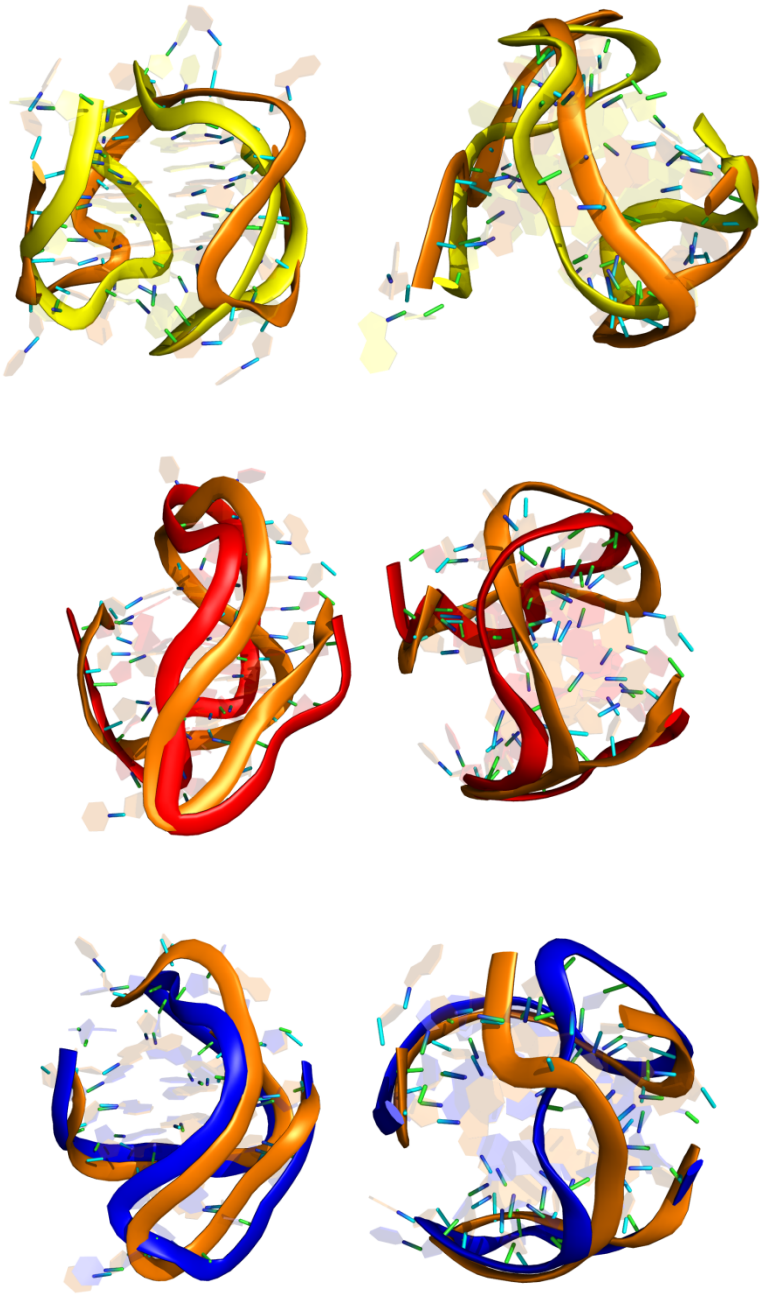

Figure S07 Two views (left and right) obtained by the RMS fit between the NMR starting structure (orange) and a representative conformation of the most populated cluster from the MD simulations **A** (top, yellow), **B** (middle, red), and **C** (bottom, blue). The RMSDs for simulations **A**, **B**, and **C** are 4.541 Å, 3.612 Å, and 2.681 Å, respectively.

The three independent simulations using three different starting structures enabled us to sample a large extension of HTS conformational space. This is in agreement with the fact that the representative conformations of simulations **A**, **B**, and **C** are slightly different, as can be observed in Fig. S08 or by comparing their cross RMSD values collected in Table S03. The representative conformation of **A** is more similar to **C**, while **B** is closer to **C**.

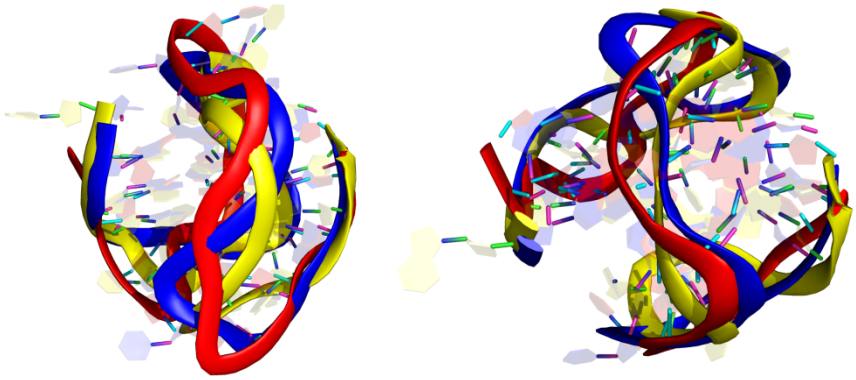

Figure S08 Two views (left and right) for the superimposition of the representative conformations of simulations **A** (yellow), **B** (red), and **C** (blue).

Table S03 Structure RMSD (Å) crossing Table with the values calculated with PyMOL.[18]

System	**A**	**B**	**C**	**ΛΛ-1-HTS**	**ΔΔ-1-HTS**
A	-	3.878	2.705	3.148	2.808
B	-	-	3.325	3.279	2.755
C	-	-	-	2.140	1.538
ΛΛ-1-HTS	-	-	-	-	1.456
ΔΔ-1-HTS	-	-	-	-	-

Interaction of ΛΛ-1 and ΔΔ-1 complexes with HTS. The experimental NMR studies indicate that the experimental NOE signals are consistent with ΛΛ-**1** binding under the diagonal loop stacked over the top quartet (Fig. 6, main text). This binding mode appears to be absent for ΔΔ-**1**. This prompted us to perform MD simulations on HTS complex associations in order to obtain further insights into this structural feature. As mentioned in the computational details, the NMR structure reported in Fig. 6 was taken as a starting binding scenario for the MD simulation of HTS with ΛΛ-**1**. This simulation is henceforth denoted as **ΛΛ-1-HTS**. We also wanted to check if ΔΔ-**1** is able to fit under the loop without causing major quadruplex structural rearrangement. The **ΔΔ-1-HTS** starting geometry was generated from **ΛΛ-1-HTS** as aforementioned, being from now denoted as **ΔΔ-1-HTS**.

As for the free HTS simulations (**A**, **B**, and **C**), the RMSD values were monitored over the simulation, using the respective unrelaxed starting structures as reference, and are plotted in Fig. 8 in the main text.

Again, the sudden jump observed in both systems is due to geometry relaxation in the force field. For the **ΛΛ-1-HTS** simulation, the inclusion of the complex does not disrupt the G-tetrads, and the complex-DNA association stabilizes during the first 5 ns of equilibration time. On the other hand, RMSD values of the diagonal loop oscillate due to the presence of the ΛΛ-**1** complex. Overall, the antiparallel basket structure is not affected and is stable for the entire 50 ns collection time. In agreement, the RMSDs between the representative conformation of this simulation and the control simulations **A**, **B**, **C** for free HTS are relatively small with values of 3.148 Å, 3.279 Å and 2.140 Å respectively which are within the variability found on the cross RMSDs of simulations **A**, **B**, and **C** (see Table S03). As seen in Fig. 9, the complex binds under the diagonal

loop with the tppz ligand stacking over the top G-tetrad, appearing to adopt a diagonal disposition over the guanine bases. This point is relevant later in this discussion.

In the **ΔΔ-1-HTS** simulation, the RMSD values converge very quickly - including the ones relative to the diagonal loop (Fig. 8), showing that ΔΔ-**1** can fit under the loop without causing major G-DNA conformational changes. Indeed, the representative conformation of the **ΔΔ-1-HTS** simulation, also represented in Fig. 8, is not much different from the **ΛΛ-1-HTS** simulation or the control simulations **A**, **B** and **C** and as might be expected the RMSDs are similar (Table S03). This resemblance is easily seen in Fig. S09 where the representative snapshots of simulations **ΛΛ-1-HTS** and **ΔΔ-1-HTS** are aligned with the NMR structure.

The main difference between the DNA association simulations is due to the relative position adopted by the ΛΛ-**1** and ΔΔ-**1** complexes inside the loop and over the G-tetrad. As mentioned earlier, ΛΛ-**1** appears more diagonally aligned whereas with ΔΔ-**1**, the stacking of the tppz ligand is more localized over two guanines of one half of the G-tetrad (see Fig. 8).

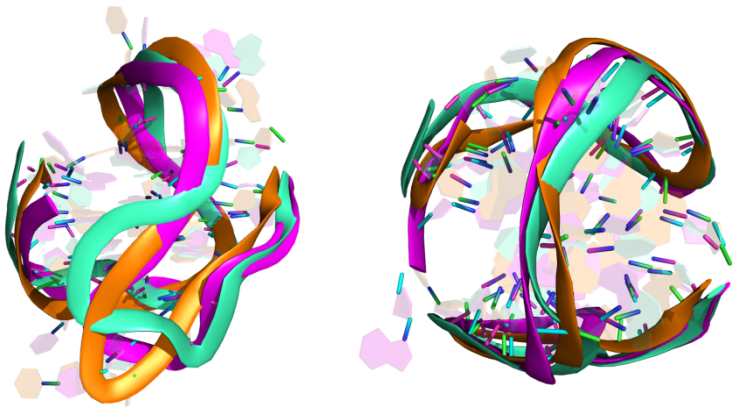

Figure S09 Representative snapshots of simulations **ΛΛ-1-HTS** (magenta), **ΔΔ-1-HTS** (aquamarine) overlapped with the NMR starting structure (orange) in side and top views

presented at left and right, respectively. The ruthenium complexes were omitted for clarity.

In order to clarify this point, a surface representation was constructed with a histogram of the positions occupied by the tpphz atoms of **ΛΛ-1-HTS** and **ΔΔ-1-HTS** (excluding the hydrogen atoms) throughout the 50 ns collection runs. These surfaces are represented in Fig. 10 and clearly show a striking difference between these simulations. In **ΛΛ-1-HTS** simulation, the tpphz is not locked and, despite being slightly diagonally aligned, is able to float over the G-tetrad interacting with the four guanines. In contrast, the tppz ligand in **ΔΔ-1-HTS** remains almost stationary over the G-tetrad and, in fact, it is even possible to observe the holes of the aromatic rings on the surface. The interaction is almost exclusively with only two guanines of the quartet, as mentioned earlier. Since the analysed ligand (tpphz) and the G-tetrad are exactly the same in both complexes, the different behavior cannot be ascribed to the intrinsic tppz:G-tetrad interaction. The different behavior is indeed caused by the different stereochemistry of the bipy ligands in the $Ru(bipy)_2$ moieties. In the **ΛΛ-1-HTS** simulation, the diagonal loop appears to be more flexible in agreement with the increased RMSD fluctuation reported in Fig 8. This means that the loop oscillations over the middle of both $Ru(bipy)_2$ moieties do not lock the association. On the other hand, in **ΔΔ-1-HTS** the loop rigidity, characterised by a low RMSD fluctuation, locks the ΔΔ-**1** complex.

With the above data, the experimental observation that ΛΛ-**1** is able to bind under the diagonal loop, stacked over a G-quartet whereas ΔΔ-**1** does not, can be rationalized by considering that both ΛΛ-**1** and ΔΔ-**1** complexes can fit under the loop, but the HTS seems to have a conformational shape consistent with the steric requirements of the ΛΛ-**1** diastereoisomer, and, if a ΛΛ-**1** complex encounters a folded HTS sequence, it may

enter inside the loop in the antiparallel basket conformation. On the other hand, the stereochemistry of ΔΔ-**1** induces too much rigidity on the loop, which perhaps prevents the complex entrance.

References

1. J. Bolger, A. Gourdon, E. Ishow and J. P. Launay, *J. Chem. Soc. Chem. Commun.*, 1995, 1799-1800.
2. M. J. Frisch, G. W. Trucks, H. B. Schlegel, G. E. Scuseria, M. A. Robb, J. R. Cheeseman, V. G. Zakrzewski, J. A. Montgomery, Jr., R. E. Stratmann, J. C. Burant, S. Dapprich, J. M. Millam, A. D. Daniels, K. N. Kudin, M. C. Strain, O. Farkas, J. Tomasi, V. Barone, M. Cossi, R. Cammi, B. Mennucci, C. Pomelli, C. Adamo, S. Clifford, J. Ochterski, G. A. Petersson, P. Y. Ayala, Q. Cui, K. Morokuma, D. K. Malick, A. D. Rabuck, K. Raghavachari, J. B. Foresman, J. Cioslowski, J. V. Ortiz, B. B. Stefanov, G. Liu, A. Liashenko, P. Piskorz, I. Komaromi, R. Gomperts, R. L. Martin, D. J. Fox, T. Keith, M. A. Al-Laham, C. Y. Peng, A. Nanayakkara, C. Gonzalez, M. Challacombe, P. M. W. Gill, B. G. Johnson, W. Chen, M. W. Wong, J. L. Andres, M. Head-Gordon, E. S. Replogle and J. A. Pople, Gaussian, Inc., Pittsburgh, PA, 2003.
3. A. D. Becke, *J. Chem. Phys.*, 1993, **98**, 5648-5652.
4. C. T. Lee, W. T. Yang and R. G. Parr, *Phys. Rev. B*, 1988, **37**, 785-789.
5. P. J. Hay and W. R. Wadt, *J. Chem. Phys.*, 1985, **82**, 270-283.
6. W. R. Wadt and P. J. Hay, *J. Chem. Phys.*, 1985, **82**, 284-298.
7. P. J. Hay and W. R. Wadt, *J. Chem. Phys.*, 1985, **82**, 299-310.
8. A. W. Ehlers, M. Böhme, S. Dapprich, A. Gobbi, A. Höllwarth, V. Jonas, K. F. Köhler, R. Stegmann, A. Veldkamp and G. Frenking, *Chem. Phys. Lett.*, 1993, **208**, 111-114.

9. J. Wang, W. Wang, P. A. Kollman and D. A. Case, *J. Mol. Graph. Modell.*, 2006, **25**, 247-260.

10. J. M. Wang, R. M. Wolf, J. W. Caldwell, P. A. Kollman and D. A. Case, *J. Comput. Chem.*, 2004, **25**, 1157-1174.

11. P. Brandt, T. Norrby, E. Akermark and P. O. Norrby, *Inorg. Chem.*, 1998, **37**, 4120-4127.

12. M.-E. Moret, I. Tavernelli and U. Rothlisberger, *J. Phys. Chem. B*, 2009, **113**, 7737-7744.

13. C. Adlhart and P. Chen, *Angew. Chem. Int. Ed.*, 2002, **41**, 4484-+.

14. I. S. Joung and T. E. Cheatham, III, *J. Phys. Chem. B*, 2008, **112**, 9020-9041.

15. I. S. Joung and T. E. Cheatham, III, *J. Phys. Chem. B*, 2009, **113**, 13279-13290.

16. W. L. Jorgensen, J. Chandrasekhar, J. D. Madura, R. W. Impey and M. L. Klein, *J. Chem. Phys.*, 1983, **79**, 926-935.

17. J. P. Ryckaert, G. Ciccotti and H. J. C. Berendsen, *J. Comp. Phys.*, 1977, **23**, 327-341.

18. W. L. DeLano, DeLano Scientific, Palo Alto, CA, USA, 2002.